Chemical Engineering Journal 385 (2020) 123963

Contents lists available at ScienceDirect

Chemical Engineering Journal

journal homepage: www.elsevier.com/locate/cej

Bidirectional anisotropic polyimide/bacterial cellulose aerogels by freeze-drying for super-thermal insulation

Xiang Zhang[a], Xingyu Zhao[a], Tiantian Xue[a], Fan Yang[a], Wei Fan[a,*], Tianxi Liu[a,b,*]

[a] State Key Laboratory for Modification of Chemical Fibers and Polymer Materials, College of Materials Science and Engineering, Innovation Center for Textile Science and Technology, Donghua University, 2999 North Renmin Road, Shanghai 201620, PR China

[b] Key Laboratory of Synthetic and Biological Colloids, Ministry of Education, School of Chemical and Material Engineering, Jiangnan University, Wuxi 214122, PR China

HIGHLIGHTS

- Bidirectional anisotropic b-PI/BC aerogels have been prepared by freeze-drying.
- The b-PI/BC aerogel shows high porosity (97.7%) and low density (46 mg cm^{-3}).
- The b-PI/BC aerogel exhibits ultra-low thermal conductivity of 23 mW m^{-1} K^{-1} in the radial direction.
- The b-PI/BC aerogel shows unique anisotropic thermal properties with an anisotropy of 2.

GRAPHICAL ABSTRACT

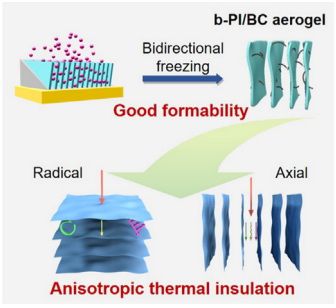

ARTICLE INFO

Keywords:
Polyimide
Aerogels
Anisotropic
Thermal insulation
Freeze-drying

ABSTRACT

There has been a growing interest in developing novel thermal insulation materials since the traditional insulation material is unable to manage heat intelligently. Herein, bidirectional anisotropic polyimide/bacterial cellulose (b-PI/BC) aerogels with good structural formability, high mechanical strength, and excellent thermal insulation properties have been prepared via bidirectional freezing technique. Polyimide makes the composite aerogels robust in mechanics, while uniform dispersion of bacterial cellulose in the aerogel can inhibit the shrinkage and retain the structural integrity, leading to higher porosity and lower density, thus reducing heat conduction throughout the whole aerogel. Due to its well-aligned lamellar structure obtained by bidirectional freezing technique, b-PI/BC aerogel exhibits distinct anisotropic thermal insulation behaviors with ultra-low thermal conductivity of 23 mW m^{-1} K^{-1} in the radial direction (perpendicular to the lamella) and nearly twice (44 mW m^{-1} K^{-1}) in the axial direction (parallel to the lamella). The anisotropy of the thermal conductivity can substantially reduce the heat transfer in the radial direction, while helps heat diffusion in-plane to avoid heat localization, which possess remarkable advantages over the random and unidirectional counterparts. Therefore, this anisotropic PI/BC aerogel can serve as a promising heat management material for practical and complex thermal insulation applications.

* Corresponding authors at: State Key Laboratory for Modification of Chemical Fibers and Polymer Materials, College of Materials Science and Engineering, Innovation Center for Textile Science and Technology, Donghua University, 2999 North Renmin Road, Shanghai 201620, PR China (T. Liu).

E-mail addresses: weifan@dhu.edu.cn (W. Fan), txliu@fudan.edu.cn, txliu@dhu.edu.cn (T. Liu).

https://doi.org/10.1016/j.cej.2019.123963
Received 17 September 2019; Received in revised form 9 December 2019; Accepted 26 December 2019
Available online 27 December 2019
1385-8947/

1. Introduction

Thermal insulation plays an important role in improving energy efficiency and reducing energy consumption worldwide [1]. Developing materials with a superior thermal insulation performance is highly desirable for many buildings and space applications where heat transfer should be strictly inhibited [2]. Aerogels as one of the typical thermal insulation materials, have attracted substantial attention recently [3]. Aerogels are obtained from gel materials, in which the solvent is replaced with gas to remain intact solid nanostructures [4]. Due to those nanoporous structures, aerogels typically exhibit low density, high porosity and low thermal conductivity. Ultra-low thermal conductivity (~20 mW m^{-1} K^{-1}) has been achieved for SiO_2 aerogels, but their widespread application is still restricted due to their brittleness as well as processing complexity [5]. Therefore, it is urgent to develop aerogels that exhibit strong mechanical strength for practical use while maintaining low thermal conductivity.

In contrast to SiO_2 aerogels, polymer aerogels show much better mechanical properties [6–8]. Among the polymer aerogels, polyimide (PI) aerogels exhibiting excellent mechanical properties and high-temperature stability have drawn much attention recently [9]. Researchers have reported a series of PI aerogels with a nanofibrous structure fabricated by supercritical carbon dioxide drying [10]. Despite showing much better mechanical strength with Young's modulus over 30 MPa, the thermal conductivity reported for PI aerogels is usually in the range of 30–60 mW m^{-1} K^{-1}, which is still higher than that of SiO_2 aerogels [11,12]. Compared with supercritical drying, freeze-drying method has several advantages, such as green, simple and inexpensive, and the porous structure can be easily adjusted by using water-soluble polyamic acid as percusor. Our previous work show that PI aerogels prepared by freeze-drying method show a thermal conductivity of 53 mW m^{-1} K^{-1} due to the large pore size formed during the freezing process [9]. Zhang et al. reported a double-cross-linking strategy to obtain a freeze-dried and robust polyimide/reduce graphene oxide/cobalt (PI/rGO/Co) aerogel, exhibiting a thermal conductivity of 40 mW m^{-1} K^{-1} [13]. However, the thermal insulation performance of PI aerogels is still inferior as comapred with traditional SiO_2 aerogels. One important reason for the inferior thermal insulation behavior of PI aerogels is the large shrinkage during the formation of PI aerogels, which results in the loss of porosity and increase of density [14,15]. Since the thermal conductivity is highly related to the porosity and porous structure, an ideal strategy for engineering the porous structure of PI aerogels is highly desirable for better thermal insulation.

The pore arrangement of aerogels is an important factor that affect the thermal insulation behaviors [16,17]. Anisotropic materials with oriented porous structure exhibit better insulation behavior than isotropic ones, since isotropic thermal insulators usually suffer from heat localization, which is not ideal for thermal management. Anisotropic aerogels can substantially reduce heat transfer and exhibit excellent insulation in a specific direction, while some heat would diffuse in another direction to avoid local heat concentration, which can increase the overall heat transfer barrier, thus resulting in improved thermal insulation compared with isotropic materials [18]. The anisotropic structure can be constructed either via top-down or bottom-up approach. Regarding the top-down approach, wood, one of the most abundant material in nature, offers an attractive platform for anisotropic material fabrication and interesting thermal behavior can be achieved via regulating anisotropic structure of wood [19]. Regarding bottom-up approach, freeze-casting is a efficient technique that enables assembly of polymer or ceramic particles into scaffolds that have a highly aligned three-dimensional porous network [20–23]. Moreover, easy control of porous structure and orientation at multiple length scales is accomplishable by modifying conditions during freeze-casting. For example, an anisotropic foam based on nanocellulose and graphene oxide has been reported with a low thermal conductivity in the radial direction by unidirectional freezing [16]. More recently, a new bidirectional freezing technique is reported, which can assemble small building blocks into a large-scale aligned and lamellar porous structure [24–27]. However, the relationship between pore arrangement and thermal insulation is not clear and a novel strategy to design porous materials for intelligent thermal insulation is highly desirable.

In this study, a lightweight, bidirectional anisotropic aerogel based on polyimide and bacterial cellulose (b-PI/BC) is reported by bidirectional freezing technique. BC with a superfine nanofibrous structure is used as a reinforcing nanofiller for PI aerogels, which would inhibit the shrinkage and retain the structural integrity of the aerogel, thus leading to higher porosity and lower density, and favoring the reduction of heat conduction and improvement of thermal insulation. Compared with random freezing and unidirectional freezing, b-PI/BC aerogel prepared by bidirectional freezing technique exhibits well-aligned lamellar porous structure. This parallel lamellar structure can substantially reduce the heat transfer in the perpendicular direction to lamella, while helps heat diffusion in-plane to avoid heat localization. The resulting b-PI/BC aerogel exhibits ultra-low thermal conductivity of 23 mW m^{-1} K^{-1} in the radial direction (perpendicular to the lamella) and nearly twice (44 mW m^{-1} K^{-1}) in the axial direction (parallel to the lamella). Such bidirectional anisotropic polymer aerogels exhibit superior thermal insulation behavior over isotropic thermal insulators, which can enable efficient thermal diffusion in the axial direction, thus resulting in improved thermal insulation over the backside in the radial direction. Therefore, lightweight, strong and anisotropic PI/BC aerogels may find practical applications as thermal insulating materials in fields of buildings and aerospace.

2. Experimental section

2.1. Materials

Bacterial cellulose membranes were purchased from Hainan Yide Food Co. Ltd. Pyromellitic dianhydride (PMDA), 4,4′-oxidianiline (ODA), triethylamine (TEA), N, N-dimethylacetamide (DMAc), alcohol (99%), and sodium hydroxide were all purchased from Sinopharm Chemical Reagent Co. Polydimethylsiloxane (PDMS, Sylgard 184) was purchased from Dow Corning Co.

2.2. Preparation of PAA/BC hydrogel

The water-soluble PAA (the precursor of PI) was produced by polycondensation of PMDA and ODA according to our previous work [28]. The BC membranes were washed with 0.1 M NaOH solution and subsequent deionized water until pH ≈ 7 followed by freeze-drying. Afterwards, 0.4 g dry BC membrane was homogenized and dispersed at high speed (18,000 rpm, IKA T25 homogenizer) for 30 min in 25 ml deionized water. Then, 1 g PAA and 1 g TEA was dissolved into the BC suspension to form a viscous PAA/BC suspension. The homogenous suspension was left for sol–gel transition at room temperature for 24 h to obtain PAA/BC hydrogel. For comparison, different amount of BC were mixed with PAA, with weight ratio to PAA of 10%, 20%, 30%, 40% and 50%, respectively.

2.3. Preparation of PI/BC aerogel via bidirectional freezing

The PAA/BC hydrogel was poured into a special square tube, which has a PDMS wedge with a slope angle of around 20° at the bottom. Then, liquid nitrogen (−196 °C) was used to freeze the bottom of the square tube through the intermediary of copper blocks. The freezing process lasted 1 h to ensure that PAA/BC hydrogel was completely frozen. Then, the sample was freeze-dried for more than 48 h at −50 °C with a freeze-dryer under 0.03 mbar pressure (Labconco Corporation, Kansas City, USA). The obtained PAA/BC aerogel was heated to 100 °C, 200 °C, and 250 °C for 60 min respectively in nitrogen flow for imidization of PAA into polyimide. The BC is stable under this thermal

treatment according to the TGA measurements (Fig. S1). Finally, the bidirectional anisotropic PI/BC composite aerogel was obtained and denoted as b-PI/BC. For comparison, PI/BC aerogels prepared by random freezing (direct freeze in liquid nitrogen) and unidirectional freezing (without PDMS wedge) were denoted as r-PI/BC and u-PI/BC, respectively.

2.4. Characterization

The morphologies of the aerogels were studied by field-emission scanning electron microscopy (FE-SEM, S-4800, Hitachi Ltd., Japan) at an acceleration voltage of 5 kV. The pore structures of the PI/BC aerogel were measured using a capillary flow porometer (CFP-1100AI, Porous Materials Inc., USA). Dispersion of bacterial cellulose in PAA aqueous solution was studied by transmission electron microscopy (TEM, JEOLJEM-2100). Thermal conductivity is measured by Hot Disk TPS 2500 S instrument (Hot Disk AB, Sweden) (see Discussion S1 and Fig. S2 for thermal conductivity measurements). Thermographic images were taken by an infrared thermal camera (TiS40, Fluke Co., Ltd, USA). Thermal stability of the aerogels was studied by thermogravimetric analyzer (F1 Libra, Netzsch Co., Ltd, German) under nitrogen atmosphere with a heating rate of 10 °C min^{-1}. Mechanical properties were tested in the compress mode by an electronic universal testing machine (UTM2102, Suns Technology Stock Co., Ltd, China) with a sensor of 100 N and the compression speed of 2 mm min^{-1}. The compressive modulus of the aerogels was tested according to the standard GB/T 1041–2008. The shrinkage of aerogels was obtained by dividing their volume by the size of the mold. The porosities of aerogels were calculated using the following equations:

$$P = (1 - \frac{\rho_0}{\rho}) \times 100\%$$

where P is the porosity, ρ_0 is the apparent density, and ρ is the skeletal density, which is estimated from a weighted average of densities of polyimide (1.4 g cm^{-3}) and BC (1.2 g cm^{-3}).

3. Results and discussions

Bacterial cellulose nanofibers were blended with poly(amic acid) (PAA) oligomer to fabricate bidirectional anisotropic PI/BC (b-PI/BC) aerogels via a sol–gel process followed by bidirectional freezing and drying, and thermal imidization, which is schematically illustrated in Fig. 1a. The digital photos of the fabrication process are also shown in Fig. S3. After high-speed homogenization, BC membrane is fragmentated and can be dispersed in aqueous solution, exhibiting a nanofibrous structure with diameter of 40–60 nm (Fig. S4a). Due to the good compatibility of hydrophilic groups on BC and carboxyl groups on PAA chains, a homogeneous PAA/BC hydrogel can be formed by blending BC with PAA, in which BC nanofibers can be dispersed uniformly (indicated by TEM image in Fig. S4b), which is the key premise for the uniform distribution of BC in aerogel. With subsequent freeze-drying and thermal imidization process, a monolith b-PI/BC aerogel can be obtained. The digital photos of as-prepared b-PI/BC aerogels with different shapes are shown in Fig. 1b. It can be seen that b-PI/BC aerogels can be designed into any desirable shapes like flowers, vases or letters by keeping detailed geometry of the molds perfectly due to a low shrinkage rate and good structural formability. As shown in Fig. 1c, the weight of an aerogel with a size of 3 cm × 3 cm × 3 cm is equal to a grain of red bean (almost 1000 times difference in volume), indicating the light-weight nature of the b-PI/BC aerogel (density of 46 mg cm^{-3}). Significantly, by using the b-PI/BC aerogel with 5 mm thick as a blocking layer between fire and a petal, the petal can retain a watery state without any visible damage or deformation after 30 min, indicating its excellent thermal insulation properties (Fig. 1d).

The microstructure of b-PI/BC aerogels is demonstrated by scanning electron microscopy (SEM) images as shown in Fig. 1e–h. By using bidirectional freezing technique, parallel arrangement of layered structure can be formed for the aerogel. Through employing polydimethylsiloxane (PDMS) wedge during freezing, ice crystals will grow both vertically away from the cold source and horizontally along the PDMS wedge due to two temperature gradients, which resulting in large-scale aligned lamellar structures as illustrated by inset in Fig. 1e (see Discussion S2 and Fig. S5 for the details of bidirectional freezing technique). For ease of illustration, we define the X-axis as radial direction and the Y-axis and Z-axis as axial direction. As demonstrated by SEM image, b-PI/BC aerogel shows a neat parallel arrangement of lamellar structure in both X-Z and X-Y cross-section with a pore size of ~10 μm and a wall thickness of 1 to 2 μm (Fig. 1e and f). The pore size distribution in both radial (Fig. S6a) and axial directions (Fig. S6b) also demonstrate the anisotropic structure of b-PI/BC aerogel. This bidirectional anisotropic structure of b-PI/BC aerogel suggests the effectiveness of bidirectional freezing technique, which favors the thermal insulation behavior. A close observation of the pore walls indicates nanoscale folds on the lamellas (Fig. 1g) and nanofibers between the lamellas (Fig. 1h), suggesting the presence of BC nanofibers in the b-PI/BC aerogel.

As the thermal conductivity is highly related to the porosity of the materials, a series of b-PI/BC aerogels with different porosities were prepared by varying the BC content. It is well known that aerogels produced by freeze-drying method are easy to suffer from severe volume shrinkage, such as for pure PI aerogel (Fig. 2a). In contrast, by adding bacterial cellulose into the polyimide matrix, shrinkage of the aerogels is inhibited obviously (Fig. 2a). With the increase of BC content, the shrinkage rate of aerogels is decreased from 36% to 17% with BC content of 40% exhibiting an optimized structural formability (Fig. 2b). This can be attributed to the fact that BC nanofibers can function as reinforcement that share the pressure of solvent removal during the drying process, and completely retain the porous structure left by ice crystal removal, resulting in lower shrinkage rate and higher structural integrity. The apparent density of b-PI/BC aerogels decreases rapidly as the content of BC raises due to the reduction in shrinkage, which is reduced to 46 mg cm^{-3} (b-PI/BC aerogel with 40% BC) from 97 mg cm^{-3} (pure PI aerogel) (Fig. 2b). The decrease of density would inevitably cause the loss of mechanical strength. However, the compressive modulus of b-PI/BC aerogel would still retain 3 MPa with a density of 46 mg cm^{-3} (Fig. S7a). Inset in Fig. 2c shows an aerogel (1 g) could withstand 2500 times of its own weight, indicating its excellent compression resistance. Besides, the mechanical strength of b-PI/BC aerogel also shows anisotropic behavior with modulus in axial direction much higher than that in radial direction (Fig. S7b). In radial direction, b-PI/BC aerogel can be compressed without fragile under more than 80% strain and recover to a certain extent after compression, indicating its elastic behavior (Movie S1). Normally, most engineered cellular materials show a scaling relationship of $E \sim \rho^n$ between Young's modulus (E) and density (ρ), where the power n of the scaling relationship depends on the material microarchitecture [29]. As for b-PI/BC aerogel, the Young's modulus is scaled with $\rho^{1.1}$ in the radial direction and $\rho^{0.5}$ in the axial direction (Fig. 2c), demonstrating a cellular-governed elastic behavior similar to that of an architecture with low density and open cell [30,31].

With the increase of BC content, the porosity also increases from 93.1% to 97.7% as shown in Fig. 2d, which facilitates a decrease in thermal conductivity. As demonstrated in Fig. 2e, the thermal conductivity (λ) of b-PI/BC aerogels, especially in the axial direction, decreases obviously as BC content increases. Two key factors are responsible for the improvement of thermal insulation performance. First, bacterial cellulose nanofiber can serve as heat barriers to hinder phonon scattering and increase interfacial thermal resistance, reducing the solid conduction of pore walls [16,32,33]. Second, bacterial cellulose nanofiber contributes to the increased porosity and decreased density. As schematically illustrated in Fig. 2f, nanofibrous structure of bacterial cellulose would serve as support between lamellas and inhibit

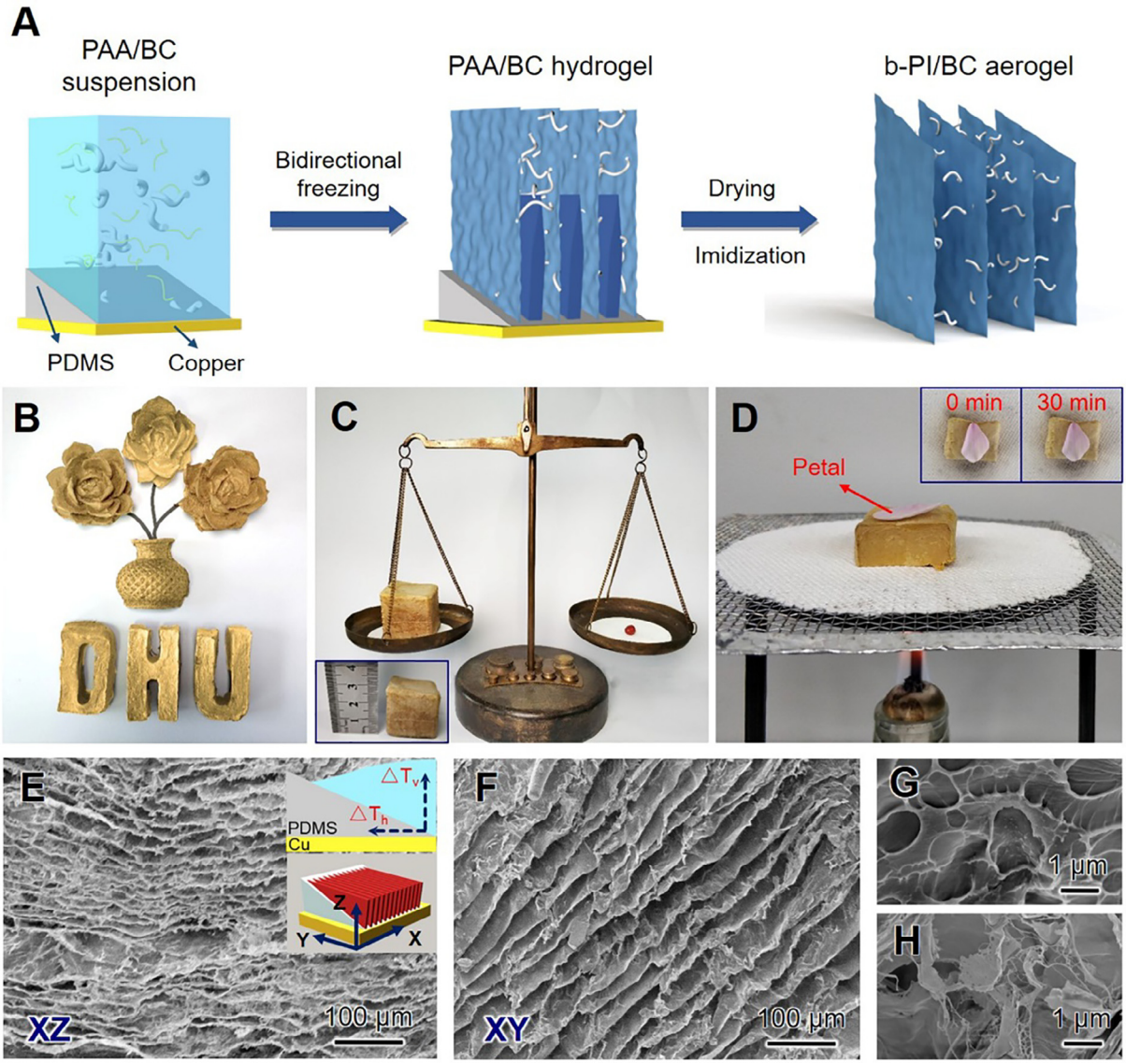

Fig. 1. Structure design and architecture of b-PI/BC aerogels. (a) Schematic illustration for preparation of b-PI/BC aerogel. (b) Photograph of b-PI/BC aerogels with different shapes like flowers, vases or letters indicating their good structural formability. (c) Photograph showing a PI/BC aerogel ($3 \times 3 \times 3$ cm^3) can keep balance with a grain of red bean, indicating its lightweight nature. (d) Photograph showing a petal of flower placed on a PI/BC aerogel can keep fresh under high temperature of alcohol lamp, showing its excellent thermal insulation performance. (e-f) SEM images of b-PI/BC aerogel in X-Z and X-Y cross-section. Inset in E indicates the temperature gradient and lamellar structure of bidirectional freezing. (g) and (h) show SEM images of pore walls at high magnifications. (For interpretation of the references to colour in this figure legend, the reader is referred to the web version of this article.)

the shrinkage during the freeze-drying process, thus leading to a perfect parallel arrangement of layered structure. The structural integrity of the pores has prevented the large mass of solid connections, allowing the heat conduction and convection of the entire materials to be reduced. In contrast, for pure PI aerogel without BC nanofibers, it will suffer from severe shrinkage due to collapse of lamellas (as shown by SEM image in Fig. S8), leading to large solid contact and increased heat conduction.

Another important factor affecting the thermal insulation behaviors is the orientation of pores in aerogels. b-PI/BC aerogels prepared by bidirectional freezing show parallel lamellar structure (Fig. 3a), which results in a large difference in the thermal conductivity in radial direction (perpendicular to the lamella) and axial direction (parallel to the lamella). As shown in Fig. 3b, the thermal conductivity of b-PI/BC aerogel is 23 mW m^{-1} K^{-1} in radial direction and 44 mW m^{-1} K^{-1} in axial direction. For comparison, PI/BC aerogels with the same composition are also prepared by random freezing (direct freezing in liquid nitrogen) and unidirectional freezing (without PDMS wedge), which are denoted as r-PI/BC and u-PI/BC, respectively. The cross-sectional SEM image of r-PI/BC aerogel shows the similar morphology in both the radial and axial direction, with both pore size of 10–20 μm and visible part of pore wall in the sampling plane (Fig. 3c). The thermal conductivities are 42 mW m^{-1} K^{-1} measured from both directions (Fig. 3d), which proves the homogeneity of aerogels in thermal insulation performance obtained by conventional random freezing method. As for u-PI/BC aerogel prepared by unidirectional freezing, it exhibits perfect cellular structures with tubular pores parallel to the freezing direction. Cross-sectional SEM image in the radial direction shows tube-like pores while it exhibits honeycomb-like pores with size of 10–20 μm in the axial direction (Fig. 3e). This u-PI/BC aerogel also shows anisotropic thermal insulation behavior, with thermal conductivity of 37 mW m^{-1} K^{-1} in the radial direction and 66 mW m^{-1} K^{-1} in the axial direction, respectively (Fig. 3f). The difference in the thermal conductivity among these three kinds of PI/BC aerogels is further explained schematically in Fig. 3g. In theory, the total thermal

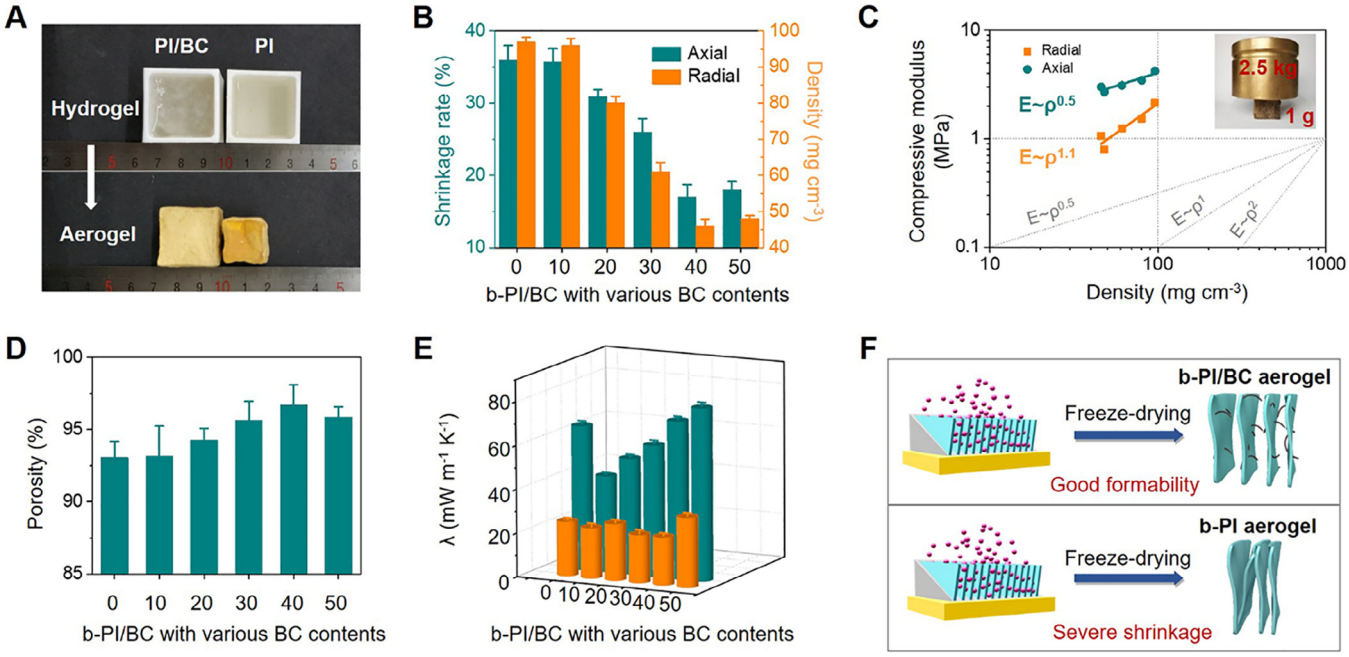

Fig. 2. Structural formability and mechanical properties. (a) Photograph of PI/BC and PI aerogels before and after freeze-drying, indicating much less shrinkage with BC as reinforcement. (b) Shrinkage rate and density of b-PI/BC aerogels with various BC contents. (c) Compressive modulus of b-PI/BC aerogels versus densities. Inset shows an aerogel (1 g) could withstand 2500 times of its own weight, indicating excellent anti-compressibility. (d) Porosity and (e) thermal conductivity (λ) of b-PI/BC aerogels with various BC contents. (f) Schematic illustrating the good structural formability of b-PI/BC aerogels, while b-PI aerogels suffer from severe shrinkage due to collapse of lamellas.

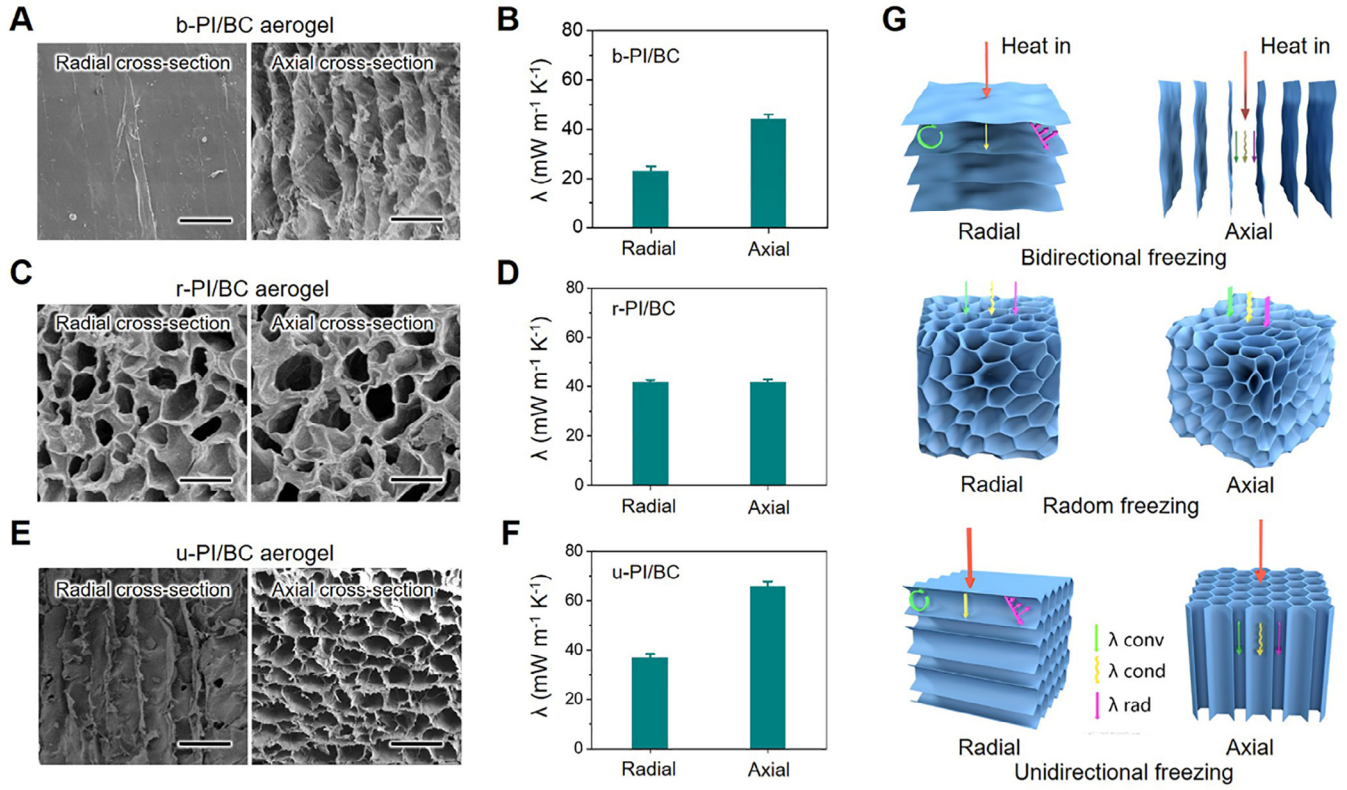

Fig. 3. Comparison of PI/BC aerogels by bidirectional, random and unidirectional freezing. (a) Radial and axial cross-sectional SEM image of b-PI/BC aerogel. (b) Thermal conductivity of b-PI/BC aerogel in radial and axial direction. (c) SEM image of r-PI/BC aerogel. (d) Thermal conductivity of r-PI/BC aerogel. (e) SEM image of u-PI/BC aerogel. (f) Thermal conductivity of u-PI/BC aerogel. (g) Schematic illustration for PI/BC aerogels prepared by bidirectional, random and unidirectional freezing for thermal insulation. The scale bar is 40 μm for all the SEM images.

conductivity of an aerogel consists of three parts: thermal convection (λ_{conv}), thermal conduction (λ_{cond}) and thermal radiation (λ_{rad}). When the thermal energy is propagated in the radial direction, lamellar structure of b-PI/BC aerogels prepared by bidirectional freezing could effectively block solid heat conduction since the interlamellar connection is missing. Moreover, the thermal convection is also restricted in the interlaminate, while the thermal radiation could be weakened by multiple refraction and emission between the regular lamellas, thus significantly reducing the total thermal conductivity. In the axial direction, heat would transfer through the gap between lamellas, resulting in higher thermal conductivity as compared with that in radial direction. As compared with r-PI/BC and u-PI/BC aerogels, the parallel lamellar structure of b-PI/BC aerogel would greatly reduce the heat transfer in the radial direction since the absence of interlamellar heat conduction. Therefore, b-PI/BC aerogel has the lowest thermal conductivity (23 mW m^{-1} K^{-1}) in comparison with r-PI/BC (42 mW m^{-1} K^{-1}) and u-PI/BC (37 mW m^{-1} K^{-1}) aerogels in the radial direction. In the axial direction, lamellar structure of b-PI/BC aerogel reduces the solid connection compared with the columnar channels of u-PI/BC aerogel, which effectively reduces the heat conduction, thus leading to lower axial thermal conductivity (44 mW m^{-1} K^{-1}) in comparison to u-PI/BC (66 mW m^{-1} K^{-1}) aerogels. Furthermore, as compared with isotropic aerogel (r-PI/BC), unique anisotropic thermal properties of b-PI/BC aerogel with an anisotropy factor of 2 can enable efficient thermal dissipation along the axial direction, thus yielding improved thermal insulation in the radial direction. Therefore, this bidirectional anisotropic PI/BC aerogel possesses remarkable advantages over the random and unidirectional counterparts.

The anisotropic thermal insulation performance of b-PI/BC is further demonstrated by infrared images. As illustrated in Fig. 4a, b-PI/BC-4 aerogels are placed on a hot stage with temperature maintaining at 180 °C along the radial and axial direction respectively. After 20 min until the sample temperature is stable, an infrared camera is used to take pictures on the side of the samples and the corresponding temperature versus the height is summarized in Fig. 4b. The results show that the temperature of the sample placed in the radial direction is much lower than that of the sample placed in the axial direction at the same height, demonstrating a much better thermal insulation performance in the radial direction. In the radial direction, the surface temperature of the sample with 25 mm thick is 30 °C, about 1/6 of the stage temperature. Moreover, by reducing the thickness of b-PI/BC aerogel from 20 mm to 5 mm, the surface temperature is still 86 °C with the stage temperature of 180 °C, indicating its excellent thermal insulation behavior even with a small thickness (Fig. 4c). The temperature change of b-PI/BC aerogel (15 mm thick) heated on a 180 °C stage for 60 min is shown in Fig. 4d. The surface temperature is only 59 °C after heating for 60 min, only slightly higher than that of initial heating, indicating its stability of thermal insulation for a long time. Fig. 4e shows the infrared images of the upper surface of aerogels under irradiation by a laser with an intensity of 1 W and a spot size of 0.5 mm. The temperature distributions on the midline of the upper surface of the aerogel are recorded in Fig. 4f. The surface temperature after radial irradiation is much higher than that of axial irradiation, which indicates that the radial direction is effective in blocking heat, while the axial direction tends to evacuate heat that would avoid heat localization. Based on this anisotropic feature, our materials can be assembled and spliced intelligently according to the environment used. b-PI/BC aerogel in axial direction can prevent heat localization for effectively blocking intense local heat source, while the aerogel placed radially can achieve excellent insulation for blocking uniform heat source. As a demonstration, two blocks of b-PI/BC aerogels are stacked together with different manners for local overheating test by the laser. As can be seen from the infrared image, when two b-PI/BC aerogels are stacked both in the radial direction, heat will be concentrated in the outermost layer and heat transfers prior in horizontal direction rather than vertical direction (Fig. 4g). In contrast, when two pieces of b-PI/BC aerogels are stacked with bottom slice placed radially and upper slice axially, the corresponding infrared image shows a temperature gradient profile with an elliptical shape since the upper slice placed axially could prevent heat localization while the bottom slice could block heat transfer efficiently, resulting in thermal insulation in the bottom side while avoid overheating in the upper side (Fig. 4h). Therefore, more effective thermal management can be achieved through reasonable combination of axial and radial b-PI/BC aerogels.

The excellent thermal insulation properties of b-PI/BC aerogels are further demonstrated by comparing it with pure PI aerogel, and commercially insulation materials like polyurethane (PU) foam and polystyrene (PS) foam. These four kinds of insulating blocks are compared by placing them on the same hot stage. A series of infrared images were taken at varied stage temperatures ranging from −40 to 160 °C, with

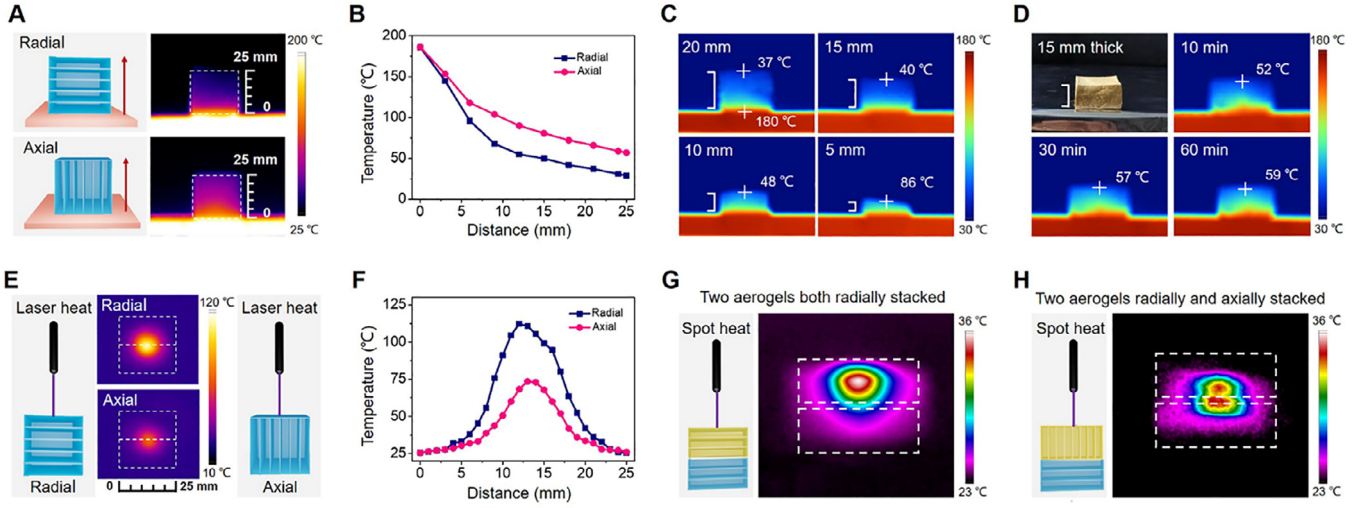

Fig. 4. Anisotropic heat transfer in b-PI/BC aerogel. (a) Infrared images of b-PI/BC aerogel on a hot stage of 180 °C in radial and axial directions indicating an anisotropic thermal insulation, and (b) the corresponding temperature at different heights in both directions. (c) Infrared images of b-PI/BC aerogels with various heights on a hot stage of 180 °C for 5 min, showing good thermal insulation at a small thickness. (d) Infrared images of b-PI/BC aerogel on a hot stage of 180 °C for 10, 30 and 60 min, indicating its long-term stability of thermal insulation. (e) Infrared images of b-PI/BC aerogel illuminated by a laser (1 W) in both directions, and (f) the corresponding temperature distribution on the midline of the surface of b-PI/BC aerogel. (g, h) Infrared images of two stacked aerogels illuminated by a laser (1 W), showing that reasonable stacking manners can offer specific thermal management.

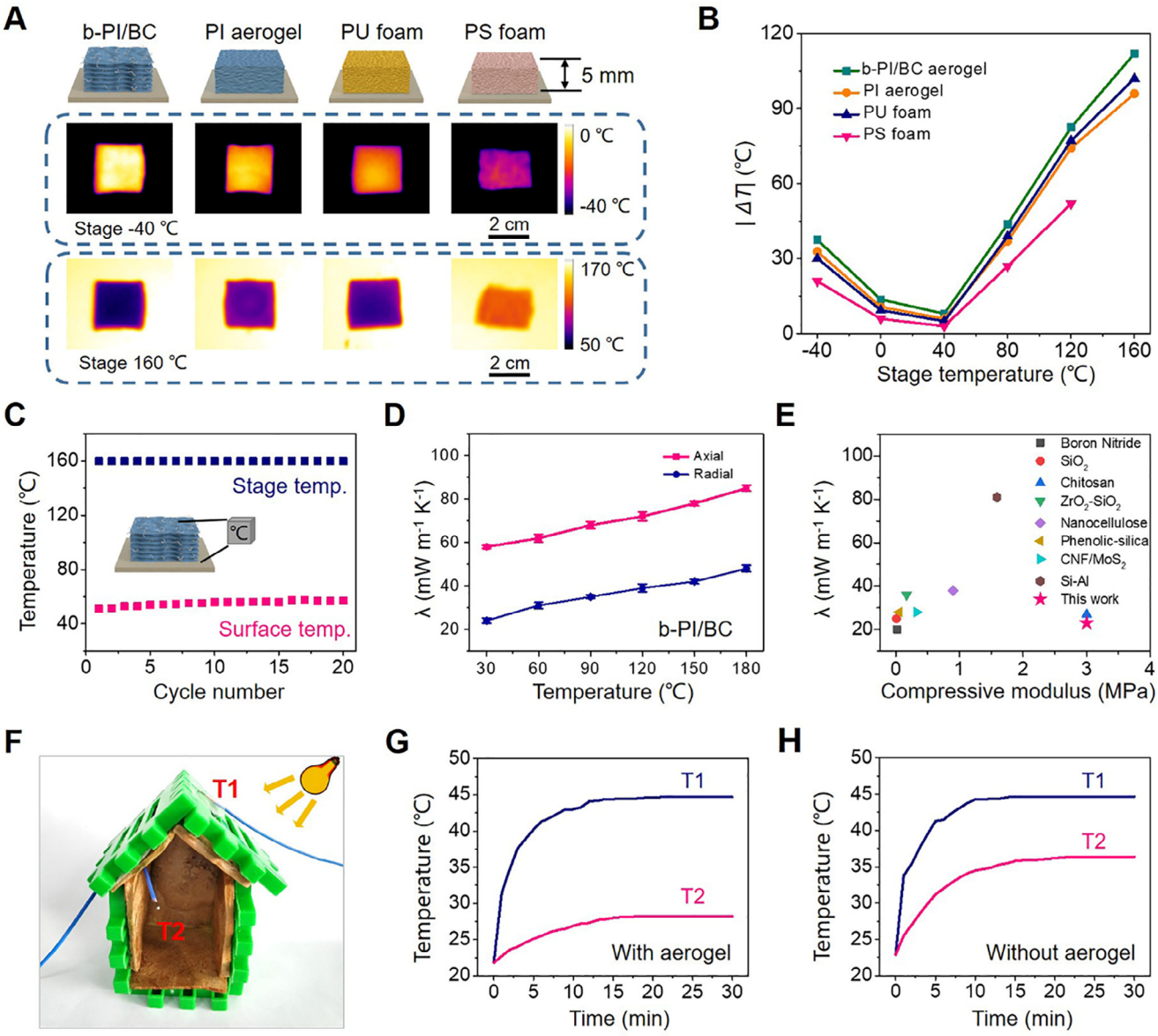

Fig. 5. Thermal insulation performance of b-PI/BC aerogels. (a) Infrared images of b-PI/BC aerogel, PI aerogel, PU foam and PS foam on a stage with −40 °C and 160 °C. (b) Temperature difference (|ΔT|) between the sample surface and the stage is plotted against the stage temperature for different samples. b-PI/BC aerogel shows higher |ΔT| at a given stage temperature, indicating better insulating behavior. (c) The upper surface temperature of b-PI/BC aerogel remains stable after repeated heating of stage to 160 °C, indicating good long-term stability as thermal insulators. (d) Thermal conductivity of b-PI/BC aerogel at different temperatures. (e) Comparison of compressive modulus and thermal conductivity of b-PI/BC aerogel with previously reported aerogel materials, including boron nitride aerogel ■ (refs. [1]), SiO_2 aerogel ● (refs. [29]), chitosan aerogel ▲ (refs. [34]), ZrO_2-SiO_2 aerogel ▼ (refs. [35]), nanocellulose aerogel ◆ (refs. [36]), phenolic-silica aerogel ◀ (refs. [37]), CNF/MoS_2 aerogel ▶ (refs. [38]), Si-Al aerogel ⬢ (refs. [39]). (f) Digital photo of the "small house" with b-PI/BC aerogel as a lining material. (g, h) The internal and external temperature changing with irradiation time by an infrared light of "small house" with and without aerogel lining. The much lower internal temperature with b-PI/BC aerogel indicates its great potential as thermal insulators for buildings.

two typical images shown in Fig. 5a with the stage temperature of −40 and 160 °C respectively. When the stage temperature is −40 °C, the upper surface temperature can remain above 0 °C for b-PI/BC aerogel, while it is below 0 °C for all the other samples with −20 °C for the PS foam. When the stage temperature is increased to 160 °C, the surface temperature of b-PI/BC aerogel can retain 48 °C, in comparison to 58 °C for PU foam and 64 °C for PI aerogel, while PS foam is melted, indicating a good thermal insulation at high temperatures for b-PI/BC aerogel. The b-PI/BC aerogels can withstand around 250 °C without decomposition by thermogravimetric analysis (TGA) (Fig. S9). The corresponding temperature difference (|ΔT|) between the sample surface and the hot stage was calculated and summarized in Fig. 5b. Larger temperature difference suggests better thermal insulation. Among the four samples, b-PI/BC aerogel always has a larger |ΔT| value than the other samples at a given stage temperature, in all the temperature range from −40 to 160 °C. More importantly, such a distinction in thermal insulation among the four samples became even more remarkable at lower or higher temperatures, suggesting that b-PI/BC aerogels can effectively block heat transfer within a considerable temperature range. The stability of thermal insulation performance of b-PI/BC aerogels is also tested by placing the aerogel on the hot stage during multiple heating–cooling cycles (Fig. 5c). After 20 cycles from room temperature to 160 °C, the upper surface of b-PI/BC aerogel still remains about 50 °C, nearly the same as the first cycle, indicating a good long-term stability as thermal insulators. Quantitatively, the thermal conductivity (λ) of the b-PI/BC aerogel in the radial direction increased slowly from

23 to 48 mW·m^{-1}·K^{-1} when the environmental temperature increased from 25 to 180 °C, indicating its good thermal insulation behavior at elevated temperatures (Fig. 5d). In comparison, for PI aerogel obtained by random freezing, the thermal conductivity rises from 57 to 84 mW·m^{-1}·K^{-1} (Fig. S10). These results indicate the superior insulating properties of the aerogel obtained by bidirectional freezing at different temperatures in the desired direction. Fig. 5e shows the comparison of thermal conductivity versus modulus of compression of b-PI/BC aerogel with previously reported silica aerogels, and some composite aerogels. The b-PI/BC aerogels exhibit excellent thermal insulation performance and mechanical properties, possessing obvious advantages as heat insulating materials.

As a proof of concept for thermal insulation applications, the as-prepared b-PI/BC aerogels are demonstrated as a lining material for building insulation. The b-PI/BC aerogel with a thickness of 5 mm was radially attached to the inside of a “small house” and irradiated by infrared light for 30 min (as shown in the digital photo in Fig. 5f). The temperatures inside (T1) and outside (T2) the “small house” were recorded by thermocouple (Fig. 5g). For comparison, the internal and external temperatures of “small house” without aerogel lining was tested under the same conditions (Fig. 5h). Even with the outside temperature more than 45 °C, the comfortable “indoor” can still remain at around 26 °C under the barrier of b-PI/BC aerogel, while the inside temperature dramatically increases to 36 °C within 10 min without aerogels, which shows the great potential of b-PI/BC aerogels as thermal insulators for practical application.

4. Conclusions

In summary, a novel class of anisotropic, mechanically robust, and lightweight PI/BC aerogel with excellent thermal insulation performance has been prepared through bidirectional freezing. Bacterial cellulose, serving as a nanofibrous reinforcement, can effectively reduce the shrinkage rate of aerogels from 36% to 17%, which greatly improves the macroscopic shape controllability and porosity of aerogel. The b-PI/BC aerogel with high porosity (97.7%) and low density (46 mg cm^{-3}) can prevent the large mass of solid connections, thus reducing the heat conduction of the entire materials, while bacterial cellulose nanofiber can increase interfacial thermal resistance, reducing the heat conduction of pore walls. Moreover, the oriented lamellar structure of b-PI/BC aerogel prepared via bidirectional freezing makes the thermal conductivity as low as 23 mW m^{-1} K^{-1} in the radial direction (perpendicular to the lamella), much lower than that (42 mW m^{-1} K^{-1}) of the aerogel obtained by random freezing. The distinct anisotropic thermal insulation behavior of b-PI/BC aerogel can yield excellent thermal insulation in the radial direction, while helps axial heat diffusion to avoid local overheating. Therefore, the b-PI/BC aerogel as a smart thermal insulator has great potential for application for complex insulation requirements in buildings, aerospace and instrumentation.

Acknowledgements

The authors are grateful for the financial support from the National Natural Science Foundation of China (21674019, 21704014), the Fundamental Research Funds for the Central Universities (2232017D-06, 2232019A3-03), Shanghai Sailing Program (17YF1400200), Shanghai Municipal Education Commission (17CG33), and Ministry of Education of the People’s Republic of China (6141A0202202)

Appendix A. Supplementary data

Supplementary data to this article can be found online at https://doi.org/10.1016/j.cej.2019.123963.

References

[1] X. Xu, Q.Q. Zhang, M.L. Hao, Y. Hu, Z.Y. Lin, L.L. Peng, T. Wang, X.X. Ren, C. Wang, Z.P. Zhao, C.Z. Wan, H.L. Fei, L. Wang, J. Zhu, H.T. Sun, W.L. Chen, T. Du, B.W. Deng, G.J. Cheng, I. Shakir, C. Dames, T.S. Fisher, X. Zhang, H. Li, Y. Huang, X.F., Double-negative-index ceramic aerogels for thermal superinsulation, Science 363 (2019) 723–727.
[2] J.Y. Zhang, Y.H. Cheng, M. Tebyetekerwa, S. Meng, M.F. Zhu, Y.F. Lu, “Stiff–soft” binary synergistic aerogels with superflexibility and high thermal insulation performance, Adv. Funct. Mater. 29 (2019) 6407–6418.
[3] R.L. Liu, X. Dong, S.T. Xie, T. Jia, Y.J. Xue, J.C. Liu, W. Jing, A.R. Guo, Ultralight, thermal insulating, and high-temperature-resistant mullite-based nanofibrous aerogels, Chem. Eng. J 360 (2019) 464–472.
[4] L.Z. Zuo, W. Fan, Y.F. Zhang, L.S. Zhang, W. Gao, Y.P. Huang, T.X. Liu, Graphene/montmorillonite hybrid synergistically reinforced polyimide composite aerogels with enhanced flame-retardant performance, Compos. Sci. Technol. 139 (2017) 57–63.
[5] S.Y. Zhao, Z. Zhang, G. Sèbe, R. Wu, R.V. Rivera Virtudazo, P. Tingaut, M.M. Koebel, Multiscale assembly of superinsulating silica aerogels within silylated nanocellulosic scaffolds: improved mechanical properties promoted by nanoscale chemical compatibilization, Adv. Funct. Mater. 25 (2015) 2326–2334.
[6] L. Zhang, H. Deng, Q. Fu, Recent progress on thermal conductive and electrical insulating polymer composites, Compos. Commun. 8 (2018) 74–82.
[7] C.Y. Liang, Z.J. Wang, Eggplant-derived SiC aerogels with high-performance electromagnetic wave absorption and thermal insulation properties, Chem. Eng. J 373 (2019) 598–605.
[8] H.Q. Guo, M.A. Meador, L. McCorkle, D.J. Quade, J. Guo, B. Hamilton, M. Cakmak, Tailoring properties of cross-linked polyimide aerogels for better moisture resistance, flexibility, and strength, ACS Appl. Mater. Interfaces 4 (2012) 5422–5429.
[9] W. Fan, X. Zhang, Y. Zhang, Y.F. Zhang, T.X. Liu, Lightweight, strong, and super-thermal insulating polyimide composite aerogels under high temperature, Compos. Sci. Technol. 173 (2019) 47–52.
[10] H.Y. Mi, X. Jing, M.A.B. Meador, H.Q. Guo, L.S. Turng, S.Q. Gong, Triboelectric nanogenerators made of porous polyamide nanofiber mats and polyimide aerogel film: output optimization and performance in circuits, ACS Appl. Mater. Interfaces 10 (2018) 30596–30606.
[11] J.Z. Feng, X. Wang, Y.G. Jiang, D.X. Du, J. Feng, Study on thermal conductivities of aromatic polyimide aerogels, ACS Appl. Mater. Interfaces 8 (2016) 12992–12996.
[12] M.A. Meador, C.R. Aleman, K. Hanson, N. Ramirez, S.L. Vivod, N. Wilmoth, L. McCorkle, Polyimide aerogels with amide cross-links: a low cost alternative for mechanically strong polymer aerogels, ACS Appl. Mater. Interfaces 7 (2015) 1240–1249.
[13] X.H. Zhang, W. Li, P.Y. Song, B. You, G. Sun, Double-cross-linking strategy for preparing flexible, robust, and multifunctional polyimide aerogel, Chem. Eng. J 381 (2020) 122784.
[14] P. Ruckdeschel, A. Philipp, M. Retsch, Understanding thermal insulation in porous, particulate materials, Adv. Funct. Mater. 27 (2017) 2256–2267.
[15] L. Cao, Q. Fu, Y. Si, B. Ding, J. Yu, Porous materials for sound absorption, Compos. Commun. 10 (2018) 25–35.
[16] B. Wicklein, A. Kocjan, G. Salazar-Alvarez, F. Carosio, G. Camino, M. Antonietti, L. Bergstrom, Thermally insulating and fire-retardant lightweight anisotropic foams based on nanocellulose and graphene oxide, Nat. Nanotechnol. 248 (2014) 277–283.
[17] J.W. Song, C.J. Chen, Z. Yang, Y.D. Kuang, T. Li, Y.J. Li, H. Huang, I. Kierzewski, B.Y. Liu, S.M. He, T.T. Gao, S.U. Yuruker, A. Gong, B. Yang, L.B. Hu, Highly compressible, anisotropic aerogel with aligned cellulose nanofibers, ACS Nano 12 (2018) 140–147.
[18] T. Li, J.W. Song, X.P. Zhao, Z. Yang, G. Pastel, S.M. Xu, C. Jia, J.Q. Dai, C.J. Chen, A. Gong, F. Jiang, Y.G. Yao, T.Z. Fan, B. Yang, L. Wågberg, R.G. Yang, L.B. Hu, Anisotropic, lightweight, strong, and super thermally insulating nanowood with naturally aligned nanocellulose, Sci. Adv. 4 (2018) 3724–3733.
[19] T. Li, Y. Zhai, S.M. He, W.T. Gan, Z.Y. Wei, M. Heidarinejad, D. Dalgo, R.Y. Mi, X.P. Zhao, J.W. Song, J.Q. Dai, C.J. Chen, A. Aili, A. Vellore, A. Martini, R.G. Yang, J. Srebric, X.B. Yin, L.B. Hu, A radiative cooling structural material, Science 364 (2019) 760–763.
[20] J.M. Wang, D. Liu, Q.X. Li, C. Chen, Z.Q. Chen, P.A. Song, J. Hao, Y.W. Li, S. Fakhrhoseini, M. Naebe, X.G. Wang, W.W. Li, Lightweight, superelastic yet thermoconductive boron nitride nanocomposite aerogel for thermal energy regulation, ACS Nano 13 (2019) 7860–7870.
[21] H. Bai, Y. Chen, B. Delattre, A.P. Tomsia, R.O. Ritchie, Bioinspired large-scale aligned porous materials assembled with dual temperature gradients, Sci. Adv. 1 (2015) 1500849.
[22] Y. Si, X.Q. Wang, C.C. Yan, L. Yang, J.Y. Yu, B. Ding, Ultralight biomass-derived carbonaceous nanofibrous aerogels with superelasticity and high pressure-sensitivity, Adv. Mater. 28 (2016) 9512–9518.
[23] C.H. Wang, X. Chen, B. Wang, M. Huang, B. Wang, Y. Jiang, R.S. Ruoff, Freeze-casting produces a graphene oxide aerogel with a radial and centrosymmetric structure, ACS Nano 12 (2018) 5816–5825.
[24] H. Bai, F. Walsh, B. Gludovatz, B. Delattre, C. Huang, Y. Chen, A.P. Tomsia, R.O. Ritchie, Bioinspired hydroxyapatite/poly(methyl methacrylate) composite with a nacre-mimetic architecture by a bidirectional freezing method, Adv. Mater. 28 (2016) 50–56.
[25] M. Yang, N.F. Zhao, Y. Cui, W.W. Gao, Q. Zhao, C. Gao, H. Bai, T. Xie, Biomimetic architectured graphene aerogel with exceptional strength and resilience, ACS Nano 11 (2017) 6817–6824.

[26] N.F. Zhao, M. Yang, Q. Zhao, W.W. Gao, T. Xie, H. Bai, Superstretchable nacre-mimetic graphene/poly(vinyl alcohol) composite film based on interfacial architectural engineering, ACS Nano 11 (2017) 4777–4784.
[27] H.L. Gao, Y.B. Zhu, L.B. Mao, F.C. Wang, X.S. Luo, Y.Y. Liu, Y. Lu, Z. Pan, J. Ge, W. Shen, Y.R. Zheng, L. Xu, L.J. Wang, W.H. Xu, H.A. Wu, S.H. Yu, Super-elastic and fatigue resistant carbon material with lamellar multi-arch microstructure, Nat. Commun. 7 (2016) 12920–12928.
[28] W. Fan, L.Z. Zuo, Y.F. Zhang, Y. Chen, T.X. Liu, Mechanically strong polyimide/carbon nanotube composite aerogels with controllable porous structure, Compos. Sci. Technol. 156 (2018) 186–191.
[29] X.Y. Zheng, H. Lee, T.H. Weisgraber, M. Shusteff, J. DeOtte, E.B. Duoss, J.D. Kuntz, M.M. Biener, Q. Ge, J.A. Jackson, S.O. Kucheyev, N.X. Fang, C.M. Spadaccini, Ultralight, ultra-stiff mechanical metamaterials, Science 344 (2014) 1373–1380.
[30] Y. Si, X.Q. Wang, L. Dou, J.Y. Yu, B. Ding, Ultralight and fire-resistant ceramic nanofibrous aerogels with temperature-invariant superelasticity, Sci. Adv. 4 (2018) 8925–8934.
[31] Z.L. Yu, N. Yang, L.C. Zhou, Z.Y. Ma, Y.B. Zhu, Y.Y. Lu, B. Qin, W.Y. Xing, T. Ma, S.C. Li, H.L. Gao, Bioinspired polymeric woods, Sci. Adv. 4 (2018) 7223–7233.
[32] G.H. Tang, C. Bi, Y. Zhao, W.Q. Tao, Thermal transport in nano-porous insulation of aerogel: factors, models and outlook, Energy 90 (2015) 701–721.
[33] G. Pernot, M. Stoffel, I. Savic, F. Pezzoli, P. Chen, et al., Precise control of thermal conductivity at the nanoscale through individual phonon-scattering barriers, Nature Mater. 9 (2010) 491–495.
[34] S.Z. Zhang, J.Z. Feng, J. Feng, Y.G. Jiang, L.J. Li, Ultra-low shrinkage chitosan aerogels trussed with polyvinyl alcohol, Mater. Des. 156 (2018) 398–406.
[35] J. He, H.Y. Zhao, X.L. Li, D. Su, H.M. Ji, H.J. Yu, Z.P. Hu, Large-scale and ultra-low thermal conductivity of ZrO_2 fibrofelt/ZrO_2-SiO_2 aerogels composites for thermal insulation Ceram, Int. 44 (2018) 8742–8748.
[36] Y. Kobayashi, T. Saito, A. Isogai, Aerogels with 3D ordered nanofiber skeletons of liquid-crystalline nanocellulose derivatives as tough and transparent insulators, Angew. Chem. Int. Ed. 53 (2014) 10394–10397.
[37] Z.L. Yu, N. Yang, V. Apostolopoulou-Kalkavoura, B. Qin, Z.Y. Ma, W.Y. Xing, C. Qiao, L. Bergstrom, M. Antonietti, S.H. Yu, Fire-retardant and thermally insulating phenolic-silica aerogels, Angew. Chem. Int. Ed. 57 (2018) 4538–4542.
[38] L. Yang, A. Mukhopadhyay, Y.C. Jiao, Q. Yong, L. Chen, Y.J. Xing, J. Hamel, H.L. Zhu, Ultralight, highly thermally insulating and fire resistant aerogel by encapsulating cellulose nanofibers with two-dimensional MoS_2, Nanoscale 9 (2017) 11452–11462.
[39] H.M. Li, Y.F. Chen, P.D. Wang, B.S. Xu, Y.B. Ma, W.B. Wen, Y.Z. Yang, D.N. Fang, Porous carbon-bonded carbon fiber composites impregnated with SiO2-Al2O3 aerogel with enhanced thermal insulation and mechanical properties, Ceram. Int. 44 (2018) 3484–3487.